Title

Simulated lesion, human observer performance comparison between thin-section dedicated breast CT images versus computed thick-section simulated projection images of the breast

Journal

Physics in Medicine and Biology, 60(8)

ISSN

0031-9155

Authors

Chen, L
Boone, JM
Abbey, CK
et al.

Publication Date

2015-04-21

DOI

10.1088/0031-9155/60/8/3347

Peer reviewed

HHS Public Access

Author manuscript

Phys Med Biol. Author manuscript; available in PMC 2016 April 21.

Published in final edited form as:

Phys Med Biol. 2015 April 21; 60(8): 3347–3358. doi:10.1088/0031-9155/60/8/3347.

Simulated lesion, human observer performance comparison between thin-section dedicated breast CT images versus computed thick-section simulated projection images of the breast

L Chen,
Department of Radiology, University of California, Davis

JM Boone,
Department of Radiology, University of California, Davis

CK Abbey,
Department of Psychology, University of California Santa Barbara

J Hargreaves,
Department of Radiology, University of California, Davis

C Bateni,
Department of Radiology, University of California, Davis

KK Lindfors,
Department of Radiology, University of California, Davis

K Yang,
Department of Radiology, University of California, Davis

A Nosratieh,
Department of Radiology, University of California, Davis

A Hernandez, and
Department of Radiology, University of California, Davis

P Gazi
Department of Radiology, University of California, Davis

Abstract

Objectives—The objective of this study was to compare the lesion detection performance of human observers between thin-section computed tomography images of the breast, with thick-section (>40 mm) simulated projection images of the breast.

Methods—Three radiologists and six physicists each executed a two alterative force choice (2AFC) study involving simulated spherical lesions placed mathematically into breast images produced on a prototype dedicated breast CT scanner. The breast image data sets from 88 patients

Corresponding Author: John M. Boone, Ph.D., Professor and Vice Chair of Radiology, UC Davis Medical Center, 4860 Y Street, Ellison Building Suite 3100, Sacramento, CA 95817, jmboone@ucdavis.edu, (916) 734-3158.

were used to create 352 pairs of image data. Spherical lesions with diameters of 1, 2, 3, 5, and 11 mm were simulated and adaptively positioned into 3D breast CT image data sets; the native thin section (0.33 mm) images were averaged to produce images with different slice thicknesses; average section thicknesses of 0.33 mm, 0.71 mm, 1.5 mm, and 2.9 mm were representative of breast CT; the average 43 mm slice thickness served to simulate simulated projection images of the breast.

Results—

Conclusions—Human observers demonstrate significantly better mass-lesion detection performance on thin-section CT images of the breast, compared to thick-section simulated projection images of the breast, when the location of the lesion is known.

Introduction

Breast cancer is the second leading cause of cancer death in women over 40 years of age. The introduction of mammographic screening has led to a significant reduction in breast cancer mortality (Andersson et al., 1988, Nyström et al., 1993). Film-based mammography has gradually been replaced with digital mammography in the United States, and currently digital mammography is used in >95 % of facilities. While mammographic screening has shown success in mortality reduction, it is known that mammography is not ideal, with reduced sensitivity for women with dense breasts. The greatest limitation of mammography is that it is a projection image modality; the anatomy in the breast is integrated along the straight-line x-ray trajectories between the x-ray source and each detector element. Consequently, the normal parenchyma of the breast can overlap and obscure cancers; this is especially problematic in women with denser breasts and, thus, cancer detection rates are generally lower in this population (Pisano et al., 2008).

To address this limitation, academic and industry-based researchers have focused on the development of a partial-angle tomographic technique called tomosynthesis, which was approved for clinical use in the United States in February 2011. Tomosynthesis makes use of similar hardware that is used for digital mammography, with the addition of some rotation of the x-ray source over a limited angular range of 15°–40°. Using limited angle reconstruction techniques, tomosynthesis provides some three-dimensional information of the breast, and has been shown to deliver an increase in detection performance when used with mammography (Park et al., 2007, Gur et al., 2009, Rafferty et al., 2013).

Other researchers have pursued the development of dedicated computed tomography of the breast (breast CT); these systems use an acquisition geometry where the patient lies prone on a table, with a single pendant breast placed through a hole in the table (Boone et al., 2001, Lindfors et al., 2008, Prionas et al., 2010, Yang et al., 2009, Shen et al., 2011, Madhav et al., 2009, Sechopoulos et al., 2010, Chen et al., 2009, Sechopoulos et al., 2008). The imaging hardware rotates 360° around the breast, capturing the data in 10–17 seconds. The geometry of the dedicated breast CT system eliminates direct exposure to the patient's thorax, as would occur if whole-body CT systems were used. The acquired data is used for full three-dimensional tomographic reconstruction of the breast, which produces tomographic images which are approximately 0.3 mm in section thickness. For the breast

CT system at our institution, the technique factors were adjusted to deliver the same radiation dose to the patient as with two-view mammography. By comparison, the thickness of the breast under standard mammography is that of the entire breast, averaging about 5 cm for the typical woman. Although tomosynthesis breast images are produced every millimeter in depth on some systems, the effective slice thickness of these images is approximately 10–20 mm thick, depending upon the size of the contrast-forming objects (Nosratieh et al., 2012).

Previous work (Packard et al., 2012) using computer-based numerical observers (a so-called pre-whitened matched filter) demonstrated superior detection performance with thin-section breast CT images compared to thick-section simulated projection images, produced by summing the entire breast CT data set. In this current work, human observers were used to compare detection performance between thin-section breast CT images and thick-section simulated projection images of the breast, which were produced by digitally averaging breast CT images. All images studied here were produced by averaging various numbers of breast CT images together, to produce different effective thicknesses ranging from the native thin-section breast CT image to a thicker image more representative of projection imaging acquisition such as with digital mammography.

Methods

Patient Selection

Patients who were determined through standard-of-care breast imaging to be diagnosed in the categories of BIRADS 4 or BIRADS 5 were approached to participate in research breast CT imaging. These patients were scheduled for needle core biopsy, and the breast CT study was performed just prior to their biopsy procedure. Informed consent was obtained through an IRB-approved and HIPAA-compliant protocol. All patients were women, with an average age of 54.5 years (σ = 10.7 years), and ranged in age from 36 to 78 years. The database of breast images used for this research was assembled from multiple clinical trials. In some trials, each breast was imaged without injected contrast agent (Lindfors et al., 2008), while in later trials both breasts of the patients were imaged with and without iodinated contrast injection (Prionas et al., 2010). All of the women in this study had suspected unilateral disease. The breast image data sets used in this investigation were non-contrast studies (*i.e.* no injected iodinated contrast), and only the unaffected breast was used (*i.e.* no suspected lesion present).

Breast CT Acquisition

The breast CT scanners at our institution were custom designed and fabricated in our laboratory. With the exception of some off-the-shelf components (*e.g.*, x-ray system, detector, motors), all components were designed, manufactured at a local machine shop, and integrated in our laboratory. These systems have been described in detail previously (Boone et al., 2005, Kwan et al., 2007), and have shown promise in terms of preliminary clinical performance (Lindfors et al., 2008, Prionas et al., 2010). The radiation dose levels were adjusted to deliver the same approximate mean glandular dose as each woman would receive during (standard) two-view mammography (Boone et al., 2004, Boone et al., 2005). The

breast CT procedure in our laboratory involves the acquisition of 500 projection (cone beam) images around 360°, requiring 16.6 seconds. During acquisition, the patient was asked to hold her breath and remain still. The patient is positioned prone, with a single breast placed into the hole on the table, where it hangs in pendent position with no compression during the scan.

After the actual acquisition procedure, the raw acquired image data were preprocessed and then used in a CT reconstruction algorithm (Feldkamp et al., 1984, Yang et al., 2007) to produce a three-dimensional volume data set of each breast scanned. In the coronal plane, the image matrix was 512×512 with pixel dimensions from 0.23–0.35 mm, depending upon the diameter of the breast. Images were reconstructed throughout the length of the breast, with between 300 and 512 images produced in each data set, depending upon the length of the breast. The slice thickness of the coronal images in each reconstructed breast CT image was 0.23 mm.

Lesion Simulation

For breast CT images, spherical lesions of various dimensions (1, 2, 3, 5, 11 mm in diameter) were inserted into the breast CT volume data set using methods reported in detail elsewhere (Packard et al., 2012). The process involves the original reconstructed volume data set, and an additional *segmented* 3D dataset of the same images. Using a previously-described algorithm (Packard and Boone, 2007), on each image, the various components inside and outside of the breast were identified using the segmentation algorithm. These components included the air outside the breast; the skin, adipose tissue, and glandular tissue were inside the breast. Glandular tissue is more dense (it appears lighter on CT images) than adipose tissue, and is essentially the same gray scale as unenhanced lesions. The lesion placement algorithm added incremental density scaled to Hounsfield units (essentially the difference in HU values between adipose tissue and glandular tissue for each individual breast image) of the displayed image to the three-dimensional voxels inside a specific spherical diameter, but only where adipose voxels were identified. Other effects such as contrast-scaling and edge blurring due to the limited spatial resolution of the system were included in the simulation (Packard et al., 2012). For the breast CT image data sets, all three cropped orthogonal views (axial, sagittal, and coronal) were displayed with the lesion centered in all three views.

The breast CT data sets were used to compute simulated projection images of the breast in this study. There are differences between these digitally-projected images and that of digital mammography; mammography has much higher spatial resolution than breast CT, and the breast is compressed during mammography acquisition; it is not compressed in the breast CT system. The differences in spatial resolution between mammography and breast CT should have little effect in this study, as all simulated lesions were sufficiently large such that spatial resolution was not an issue. Hence, this study is applicable to mass lesions and not to lesions which present only with microcalcifications. While the simulated projection images used in this study were produced by averaging breast CT images over an appreciable volume (average thickness >40 mm), the simulated projection images here were not

acquired under breast compression as in an actual digital mammography system. The role of breast compression on lesion conspicuity was not addressed in this study.

Mammography also involves an x-ray spectrum which is much lower in effective x-ray energy (*e.g.*, 26 kV spectrum from Mo/Mo anode/filter tube) than that used in breast CT (80 kV spectrum). To address this, the segmented breast CT data sets were assigned effective linear attenuation coefficients (Boone and Chavez, 1996) for air, skin, glandular tissue, adipose tissue, and the added simulated lesion components, corresponding to that of a 26 kV x-ray spectrum (Boone and Seibert, 1997). These 5 component data sets were then summed in the computer to produce simulated cranial caudal (axial) and sagittal simulated projection images. For the thick-slice images which emulate simulated projection images of the breast, two view images were presented; axial and sagittal. The production of a coronal image is not possible in projection mammography, as it would require imaging through the thorax of the patient.

Two Alternative Forced Choice Experiment

Software was written which executed the 2 alternative forced choice (2AFC) human observer tests. The 2AFC procedure involved showing each human observer two sets of images; one set on the left, and another set on the right side of the display. One of the sets contained a lesion, the other set did not. Because the lesions were inserted synthetically, “truth” as to lesion presence or absence was explicitly known. Examples of the images displayed are shown in Figure 1. The observer was asked to select which data set contained the inserted lesion. The observer pressed either the left arrow or right arrow key on a standard keyboard to indicate whether they thought they lesion was on the left or right side of the display. For breast CT data sets, three orthogonal images (coronal, sagittal, and axial) of the volume of interest inside the breast were displayed on each side of the presentation. The lesion (if present) was centered in these regions of interest, and small red hash marks were placed to indicate the central location of the lesion in all 3 orthogonal views. For the thick section simulated projection images, coronal images are not possible, and each image set included sagittal and axial images only.

Viewing distance and time to make a decision were not constrained in this study. Observers were given feedback after each response: a green circle indicated that the choice was correct, and a red circle indicated that the choice was incorrect. Observer performance studies were conducted with room lights dimmed, on a variety of computer systems all of which utilized flat-panel display technology (2560 × 1600 pixel Samsung SyncMaster 305T, Seoul, South Korea) appropriate for image viewing. The performance characteristics of this monitor were measured (luminance versus gray scale) and were found to be typical of modern medical display technology, however the gray scale was not explicitly calibrated to the DICOM 14 Standard (GSDF). Nevertheless, the experienced radiologist reviewers were comfortable with the gray scale presentation of the monitor. The readers were not able to adjust the window / level settings on the computer display.

A total of 88 breast CT data sets were used for this study, and each data set was reused at different locations within each breast data set 4 times during each test, producing 352 image pairs. Each observer evaluated these data sets over a range of other parameters, including 5

lesion diameters and 5 different slice thicknesses (4 breast CT slice thicknesses, and the projection image data set). A subset of 13 of these combinations was studied. Thus, each observer viewed 4576 pairs of image data (each containing either 2 or 3 images), comprising over 20,000 small images. If an observer averaged 10 seconds per decision, the entire process would require 12.8 hours. After each observer's response, feedback was given in the form of a small green or red circular indicator. Feedback was used to help the observers remain vigilant and keep a constant level of performance.

After each study, the proportion of correct responses (PC) was computed. It is a well-established result of receiver operating characteristic (ROC) curve analysis (Swets, 1988) that PC is equivalent to the area under the ROC curve (AUC) for 2AFC studies. In this regime, pure guessing would result in 50 % correct on average, and therefore the scores range from 50 % to 100 % correct.

A total of 3 board certified radiologists, each subspecialty-trained in breast imaging, completed the testing. The three radiologists had 1.5, 2.5, and 31 years of post-fellowship experience in breast imaging. Radiologist performance was computed as the mean and standard deviation of this group. A total of 6 medical physicists also completed the human observer tests, including 2 faculty and 4 senior graduate students. Most observers performed this analysis spanning over several days.

Two Alternative Forced Choice Analysis

The simple calculation of percent correct (PC) is equivalent (Burgess, 1995) in this case to the area under an ROC curve (AUC), which is an often-used metric for observer performance analysis (Burgess, 1995). In this study, PC was known for both the human observer, PC_{Obs}, and for the pre-whitened matched filter ideal observer, PC_{PWMF}. To calculate the efficiency of the human observer, the detectability index, d', was computed for each observer according to the formula

$$d' = \sqrt{2}\Phi^{-1}(PC), \quad (1)$$

where $\Phi(x)$ is the cumulative normal distribution function. The relative efficiency, η, was determined from the ratio of squared d' values:

$$\eta = \left(\frac{d'_{\mathrm{OBS}}}{d'_{\mathrm{PWMF}}} \right)^2. \quad (3)$$

Breast Density

All of the 88 breast CT data sets were previously segmented and the average glandular fraction (AGF) was computed for each breast (Packard and Boone, 2007). The AGF is computed as the ratio of the glandular tissue volume to the overall volume of the breast. The AGF for each of the 88 breast data sets was used to rank-order the data set, as an objective measure of breast density. To assess performance differences as a function of breast density in this study, the results from the 50 % of breasts with the highest AGF were averaged, and

compared against the average performance achieved on the 50 % of breasts with the lowest AGF.

Statistical Methodology

Clinical validations of imaging systems often rely on multi-reader multi-case experimental designs that allow for generalization to the population of readers and cases. In this investigation, we have a total of three radiologists, which is not sufficient for generalizing to the population of readers. As a result, we pursue a within-subjects design where performance effects are tested for each radiologist. Significance is defined as a family-wise error rate of 0.05 correcting for multiple comparisons over the three radiologist readers.

In each forced choice experiment, readers responded to 4 different trials derived from each of the 88 patient scans for a total of 352 trials. Each trial was scored 1 if the observer selected the target-present alternative and 0 if they selected the target-absent alternative. The 4 scores from each case were averaged into a single case score for each reader. Inference was performed using paired *t*-test comparisons across these 88 cases scores in different conditions. All tests were two-sided with $df = 87$. Corrections for multiple comparisons were implemented as described above.

Results

Display screens for the human observer performance experiments are illustrated in Figure 1. Figure 1a illustrates the screen comparing CT images, where the 3 orthogonal images (coronal, sagittal, axial) are shown simultaneously. The lesion, if present, was located in the center of each of the images, all of whom share one common voxel. Figure 1b illustrates the comparisons for the simulated projection images, where only 2 images (axial and sagittal) are shown.

Figure 2 illustrates the primary results of this investigation. The pre-whitened matched filter (PWMF) “ideal-observer” results were determined in a previous study (Packard et al., 2012), and are included here for comparison. For the thin slice (CT) images, the radiologist observers demonstrated performance similar to the PWMF observer for lesions, except for the 1 mm diameter lesion. The radiologist observer performance came closer to that of the ideal observer for the CT images, in comparison to the synthetic simulated projection images. Overall, the trends in performance for the PWMF observer, radiologists, and physicist observers, were similar. Statistical analysis of lesion size finds significant improvements in performance (family-wise $p < 0.05$) with a 0.71 mm average slice thickness compared to the simulated projection images for all lesion sizes above 1 mm. At the 1 mm lesion size, the difference was significant for one reader, but not significant for the other two.

Relative efficiency defines the performance of a human observer relative to the ideal observer, and Figure 3 illustrates the relative efficiency of the radiologists for both the thin-section CT images and the thick-section simulated projection images. These data clearly illustrate that radiologists are more efficient in detection of lesions on the thin slice CT images that do not have overlapping tissue, than they are in detecting lesions on projection

image data. This observation has practical implications with respect to clinical breast imaging.

Breast density is known to have a significant impact on observer detection performance. Figure 4 illustrates the radiologist observer performance for both thin-section (CT) and thick-section simulated projection images. Considerable differences in performance as a function of breast density are seen in Figure 4 for both CT and simulated projection images. Except for the largest 11 mm diameter lesion, the radiologists' detection performance in dense breasts with breast CT imaging outperformed that in the fatty breast for simulated projection images, demonstrating that breast CT may partially (but substantially) mitigate the influence of breast density in regards to reducing sensitivity, compared to projection imaging of the breast.

For all 3 observer types (ideal, radiologists, and physicists) performance in lesion detection degrades as the thickness of the breast images increases when 2 mm simulated lesions were used (Figure 5). For the 2 mm lesion size, all sectional images (0.33 mm to 0.29 mm average section thickness) lead to significantly higher performance than simulated projection images for all three readers.

Discussion

The results of this investigation clearly demonstrate that human observers are better able to identify synthetic spherical lesions in physically-measured breast parenchyma backgrounds when thin section (breast CT) images are used, in comparison to thick-section simulated projection images. This observation suggests that the use of breast CT may increase performance levels in mass-lesion detection over planar 2-D simulated projection images of the breast.

Figure 1 illustrates both breast CT and simulated projection images that were used in the two alternative forced choice experiments performed for this investigation. It is noted that the breast CT images and simulated projection images have fundamentally different noise texture, and it is likely that this is the primary basis for the difference in detection performance between the thin section breast CT images (Figure 1a) and the thick section simulated projection images seen in Figure 1b. A previous study (Chen et al., 2012, Chen et al., 2013) showed that a measure of anatomical noise texture, β, was significantly different between breast CT ($\beta \approx 1.8$) and simulated projection images of the breast (where $\beta \approx 2.8$ to 3.2). The theoretical basis for this difference in β was derived in earlier work (Metheany et al., 2008).

With respect to the early detection of breast cancer using image-based screening methods, two important observations are evident from this study: (1) the PWMF observer performs significantly ($p<0.05$) better on thin section images than on thick section images, and (2) radiologists perform closer to the PWMF observer with thin section images, as compared to thick section images ($p<0.05$). This latter observation is further emphasized by the differences in relative efficiency shown in Figure 3 between CT and simulated projection images. The combination of these observations leads to a significant improvement of

detection performance on thin-section breast CT images compared to thick-section, simulated projection images of the breast. Figure 2 illustrates that both the PWMF observers and human observers demonstrate better detection performance with thin slice images (bCT) compared to simulated projection images, and it is not surprising that detection performance degrades as the size of the lesion decreases. The greater efficiency of radiologists for thin-section images (Figure 3) is likely due to the problem of tissue overlap which occurs for the thicker simulated projection images. We postulate that humans are more challenged by tissue overlap than computer observers, and consequently perform better (are more efficient) when tissue overlap is reduced as with CT images. In a sense, this is the *power of tomography*.

When the data are evaluated based on breast density (Figure 4), thin section imaging with dense breasts outperforms projection imaging of fatty-replaced breasts, for lesion diameters 8 mm or less. The cross-over seen in Figure 4 occurs because the large 11 mm lesions are simply quite visible in fatty-replaced breasts on both breast CT and simulated projection images. These data suggest that thin section imaging may potentially mitigate some of the loss in performance of projection imaging in the dense breast. With the recent emphasis of legislation in the United States in regards to the dense breast, these findings are timely and demonstrate that breast CT is able to deliver better lesion detection in the dense breast than simulated projection imaging.

Figure 5 shows a considerable reduction in human observer performance for both radiologists and physicists for the thinnest section (0.33 mm), compared to the slightly thicker (0.71 mm) images. We postulate that this drop in performance is due to the increase in x-ray quantum noise associated with these low-dose, very thin section images. It is noted that the radiation dose levels in the breast CT protocols were designed to approximate the same dose levels that the women would receiving during two-view mammography. While anatomical noise appears to limit the performance of human observers in section thicknesses greater than 1 mm, it appears that quantum noise becomes the more dominant distractor for the thinnest breast CT images. This is consistent with the findings of Burgess, *et Al*., where he and colleagues found that quantum noise was only important for the smallest of lesions, precisely those 1 mm in diameter or smaller.

Limitations

There are limitations with this study. The breast images were produced from actual breast CT scans of human patients, however the spherical lesions were computer synthesized and inserted into the breast images. The technique for lesion insertion was developed with attention to detail, and includes realistic models for spatial resolution loss and quantum noise; it is described in detail in Packard, *et Al*. It is also noted that the lesion insertion was performed using the exact same algorithm for both simulated projection images and in the volumetric CT data sets, so these limitations may balance out in the final comparisons.

The observer performance paradigm was “signal known exactly” (SKE), where the observer knows exactly where the lesion is, if present, is located. This SKE method for assessing observer performance is a widely used method for evaluating and comparing human

observer performance. It is well acknowledged, however, that the results of SKE human observer experiments generally over-estimate the detection performance than the real-world situation where search is a key factor in lesion detection. While the overall performance levels in SKE experiments are likely to be higher than with search-based observer detection studies, the emphasis in this paper is the comparison between images of different thicknesses using the same observer performance methods. It is anticipated that if a search paradigm approach was used, the comparative results would be similar (in a relative sense) to those presented in this paper.

Additionally, the thick-section simulated projection images were computed by summing thin-section breast CT images. While these images do have the appearance of mammograms and the process of computing them is physically consistent with actual mammography, the spatial resolution of our images is lower than mammography and the breasts were not compressed as with mammography. Finally, this study addressed only non-contrast enhanced mass lesions. The identification of microcalcifications is an important aspect of breast cancer detection and this aspect of performance was not addressed in this study.

Conclusions

A previous investigation showed that the ideal observer (PWMF) demonstrated better detection performance on thin section images (breast CT) compared to simulated projection images of the breast. This study demonstrated that human observers also perform better for a simple lesion detection task in thin-section breast CT images compared to simulated projection images of the breast. Importantly, radiologists show significantly better efficiency in their interpretation of thin section images, compared to simulated projection images. These findings suggest that for soft-tissue mass lesions, breast CT may produce superior detection performance, compared to mammography, in the breast cancer screening environment.

Acknowledgements

This work was funded in part by a grant from the National Institutes of Health (NIH R01 EB002138).

References

Andersson I, Aspegren K, Janzon L, Landberg T, Lindholm K, Linell F, Ljungberg O, Ranstam J, Sigfusson B. Mammographic screening and mortality from breast cancer: the Malmo mammographic screening trial. BMJ. 1988; 297:943–948. [PubMed: 3142562]

Boone JM, Chavez AE. Comparison of x-ray cross sections for diagnostic and therapeutic medical physics. Med Phys. 1996; 23:1997–2005. [PubMed: 8994164]

Boone JM, Kwan AL, Seibert JA, Shah N, Lindfors KK, Nelson TR. Technique factors and their relationship to radiation dose in pendant geometry breast CT. Med Phys. 2005; 32:3767–3776. [PubMed: 16475776]

Boone JM, Nelson TR, Lindfors KK, Seibert JA. Dedicated breast CT: radiation dose and image quality evaluation. Radiology. 2001; 221:657–667. [PubMed: 11719660]

Boone JM, Seibert JA. An accurate method for computer-generating tungsten anode x-ray spectra from 30 to 140 kV. Med Phys. 1997; 24:1661–1670. [PubMed: 9394272]

Boone JM, Shah N, Nelson TR. A comprehensive analysis of DgN(CT) coefficients for pendant-geometry cone-beam breast computed tomography. Med Phys. 2004; 31:226–235. [PubMed: 15000608]

Burgess AE. Comparison of receiver operating characteristic and forced choice observer performance measurement methods. Med Phys. 1995; 22:643–655. [PubMed: 7643805]

Chen L, Abbey CK, Boone JM. Association between power law coefficients of the anatomical noise power spectrum and lesion detectability in breast imaging modalities. Phys Med Biol. 2013; 58:1663–1681. [PubMed: 23422272]

Chen L, Abbey CK, Nosratieh A, Lindfors KK, Boone JM. Anatomical complexity in breast parenchyma and its implications for optimal breast imaging strategies. Med Phys. 2012; 39:1435–1441. [PubMed: 22380376]

Chen Y, Liu B, O'connor JM, Didier CS, Glick SJ. Characterization of scatter in cone-beam CT breast imaging: comparison of experimental measurements and Monte Carlo simulation. Med Phys. 2009; 36:857–869. [PubMed: 19378746]

Feldkamp LA, Davis LC, Kress JW. Practical cone-beam algorithm. J. Opt. Soc. Am. A. 1984; 1:612–619.

Gur D, Abrams GS, Chough DM, Ganott MA, Hakim CM, Perrin RL, Rathfon GY, Sumkin JH, Zuley ML, Bandos AI. Digital Breast Tomosynthesis: Observer Performance Study. Am. J. Roentgenol. 2009; 193:586–591. [PubMed: 19620460]

Kwan ALC, Boone JM, Yang K, Huang SY. Evaluation of the spatial resolution characteristics of a cone-beam breast CT scanner. Medical Physics. 2007; 34:275–281. [PubMed: 17278513]

Lindfors KK, Boone JM, Nelson TR, Yang K, Kwan AL, Miller DF. Dedicated breast CT: initial clinical experience. Radiology. 2008; 246:725–733. [PubMed: 18195383]

Madhav P, Crotty DJ, Mckinley RL, Tornai MP. Evaluation of tilted cone-beam CT orbits in the development of a dedicated hybrid mammotomograph. Phys Med Biol. 2009; 54:3659–3676. [PubMed: 19478374]

Metheany KG, Abbey CK, Packard N, Boone JM. Characterizing anatomical variability in breast CT images. Med Phys. 2008; 35:4685–4694. [PubMed: 18975714]

Nosratieh A, Yang K, Aminololama-Shakeri S, Boone JM. Comprehensive assessment of the slice sensitivity profiles in breast tomosynthesis and breast CT. Med Phys. 2012; 39:7254–7261. [PubMed: 23231276]

Nyström L, Wall S, Rutqvist LE, Lindgren A, Lindqvist M, Rydén S, Andersson J, Bjurstam N, Fagerberg G, Frisell J, Tabár L, Larsson LG. Breast cancer screening with mammography: overview of Swedish randomised trials. The Lancet. 1993; 341:973–978.

Packard, N.; Boone, JM. Glandular segmentation of cone beam breast CT volume images. Jiang, H.; Michael, JF., editors. SPIE; 2007. p. 651038

Packard NJ, Abbey CK, Yang K, Boone JM. Effect of slice thickness on detectability in breast CT using a prewhitened matched filter and simulated mass lesions. Med Phys. 2012; 39:1818–1830. [PubMed: 22482604]

Park JM, Franken EA, Garg M, Fajardo LL, Niklason LT. Breast Tomosynthesis: Present Considerations and Future Applications. RadioGraphics. 2007; 27:S231–S240. [PubMed: 18180229]

Pisano ED, Hendrick RE, Yaffe MJ, Baum JK, Acharyya S, Cormack JB, Hanna LA, Conant EF, Fajardo LL, Bassett LW, D'orsi CJ, Jong RA, Rebner M, Tosteson AN, Gatsonis CA. Diagnostic accuracy of digital versus film mammography: exploratory analysis of selected population subgroups in DMIST. Radiology. 2008; 246:376–383. [PubMed: 18227537]

Prionas ND, Lindfors KK, Ray S, Huang SY, Beckett LA, Monsky WL, Boone JM. Contrast-enhanced dedicated breast CT: initial clinical experience. Radiology. 2010; 256:714–723. [PubMed: 20720067]

Rafferty EA, Park JM, Philpotts LE, Poplack SP, Sumkin JH, Halpern EF, Niklason LT. Assessing Radiologist Performance Using Combined Digital Mammography and Breast Tomosynthesis Compared with Digital Mammography Alone: Results of a Multicenter, Multireader Trial. Radiology. 2013; 266:104–113. [PubMed: 23169790]

Sechopoulos I, Feng SS, D'orsi CJ. Dosimetric characterization of a dedicated breast computed tomography clinical prototype. Med Phys. 2010; 37:4110–4120. [PubMed: 20879571]

Sechopoulos I, Vedantham S, Suryanarayanan S, D'orsi CJ, Karellas A. Monte Carlo and phantom study of the radiation dose to the body from dedicated CT of the breast. Radiology. 2008; 247:98–105. [PubMed: 18292479]

Shen Y, Yi Y, Zhong Y, Lai CJ, Liu X, You Z, Ge S, Wang T, Shaw CC. High resolution dual detector volume-of-interest cone beam breast CT--Demonstration with a bench top system. Med Phys. 2011; 38:6429–6442. [PubMed: 22149826]

Swets JA. Measuring the accuracy of diagnostic systems. Science. 1988; 240:1285–1293. [PubMed: 3287615]

Yang D, Ning R, Cai W. Circle Plus Partial Helical Scan Scheme for a Flat Panel Detector-Based Cone Beam Breast X-Ray CT. International Journal of Biomedical Imaging. 2009; 2009

Yang K, Kwan AL, Boone JM. Computer modeling of the spatial resolution properties of a dedicated breast CT system. Med Phys. 2007; 34:2059–2069. [PubMed: 17654909]

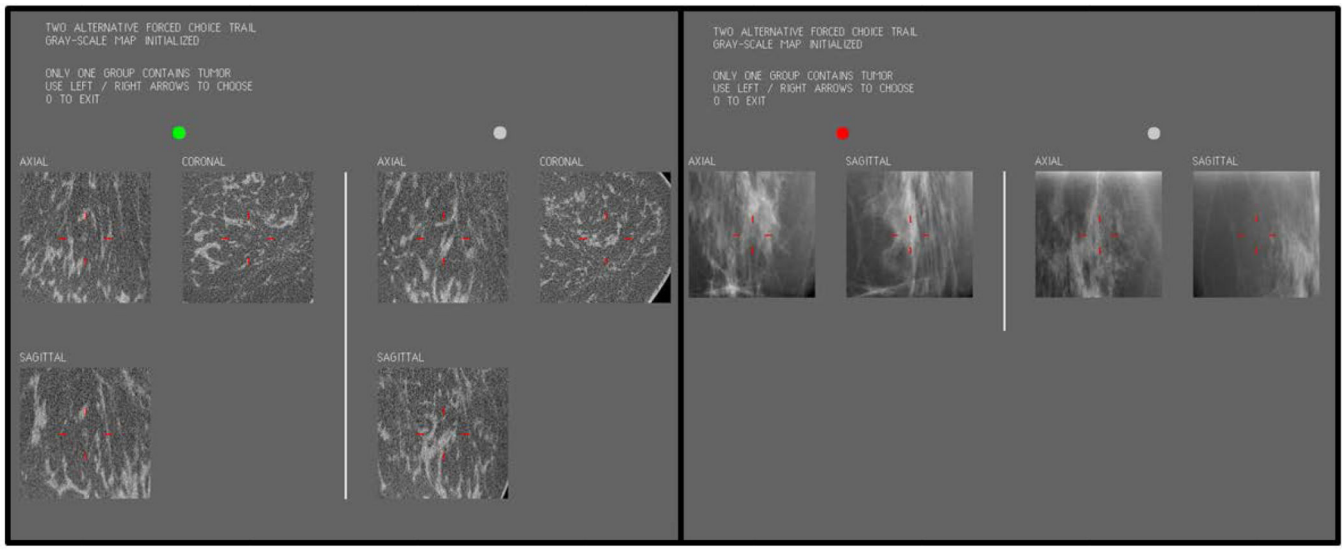

(a) (b)

Figure 1.

a: An example of the screen shown to human observers for thin-section images (CT) is illustrated.

b: The screen shot to human observers for thick-section simulated projection images is shown.

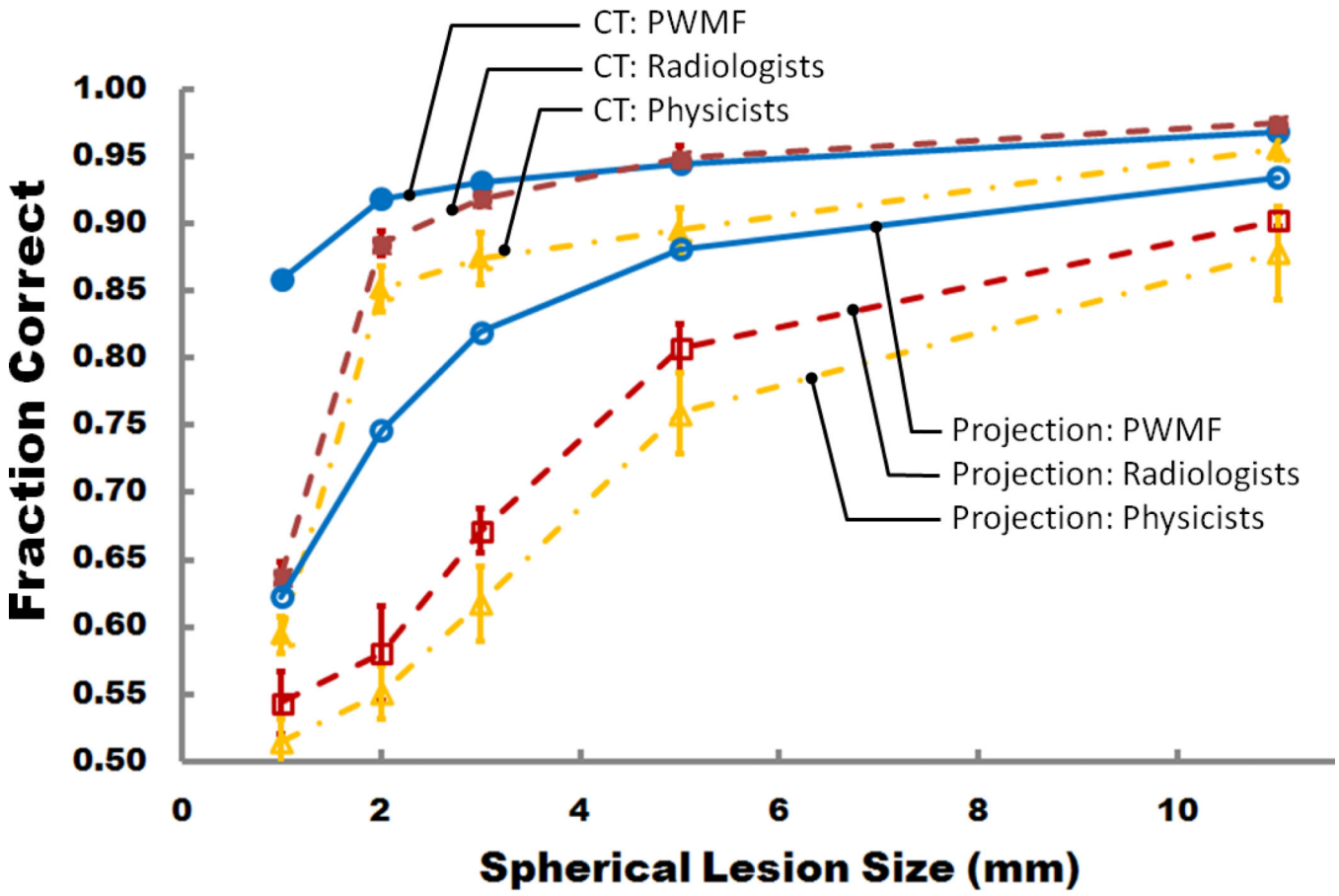

Figure 2.

Observer performance (fraction correct) as a function of lesion diameter is illustrated. Results for the PWMF (pre-whitened matched filter) observer, radiologists, and physicists are shown for both thin-section (CT) and thick-section simulated projection images.

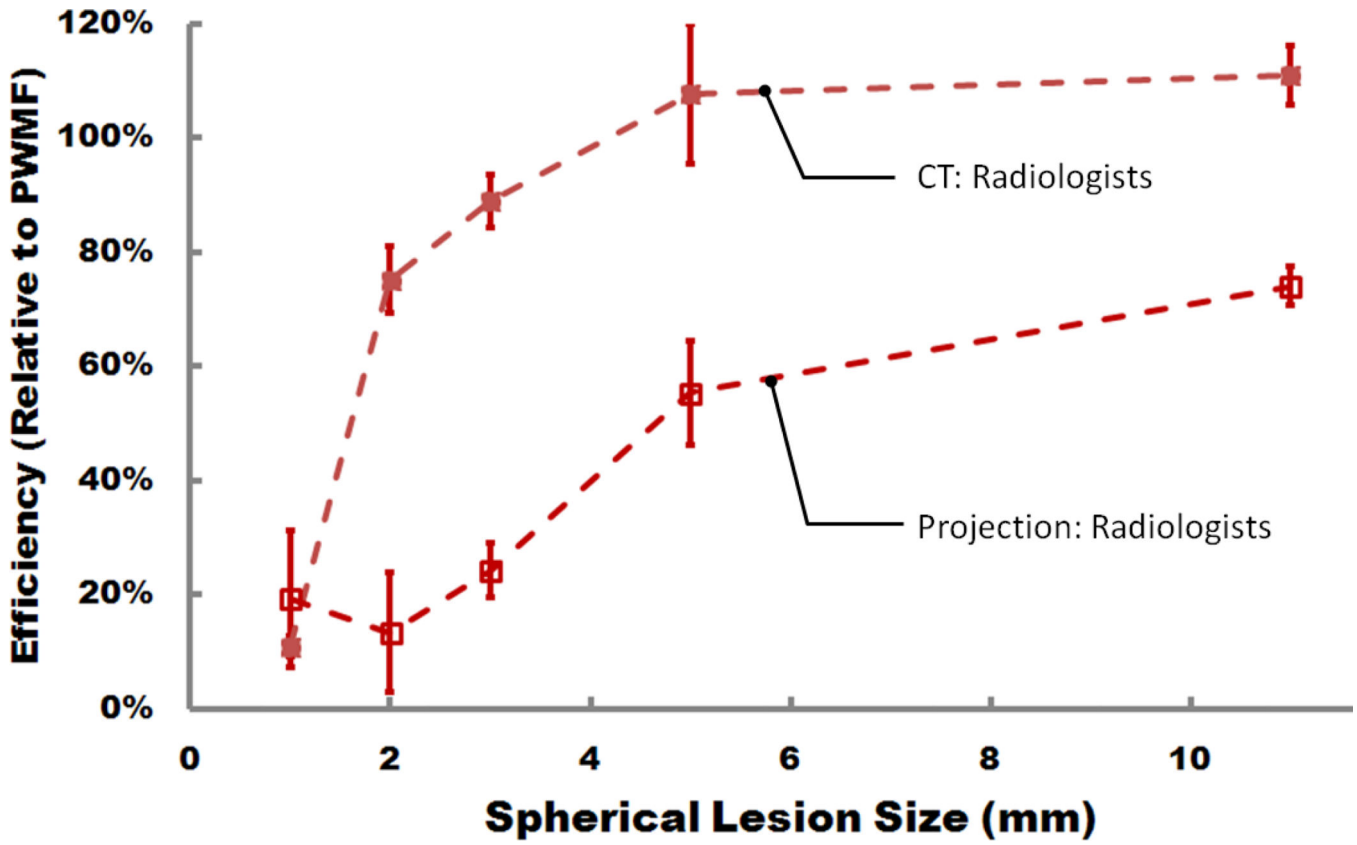

Figure 3.
The relative efficiency of radiologists is shown in comparison to the PWMF observer. Radiologists are more efficient at extracting data from CT images than from thick-section simulated projection images.

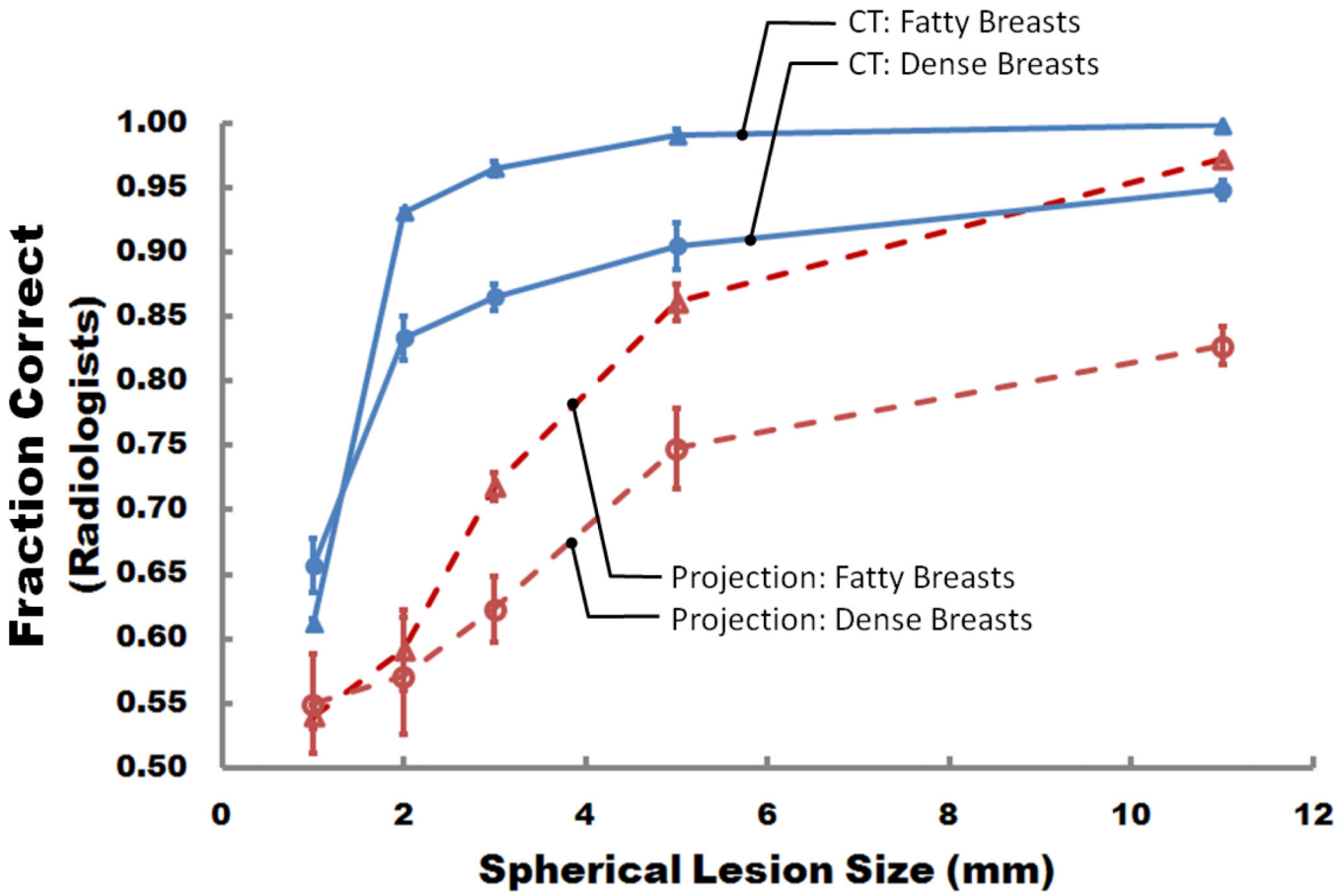

Figure 4.

Human observer performance for radiologists is illustrated as a function of simulated lesion diameter. Here, the data was separated by volume glandular fraction (breast density). The results labeled “fatty” breasts represent observer performance for breasts with lower than median density, while results labeled “dense” breasts represent observer performance for breasts with computer-determine densities greater than the median.

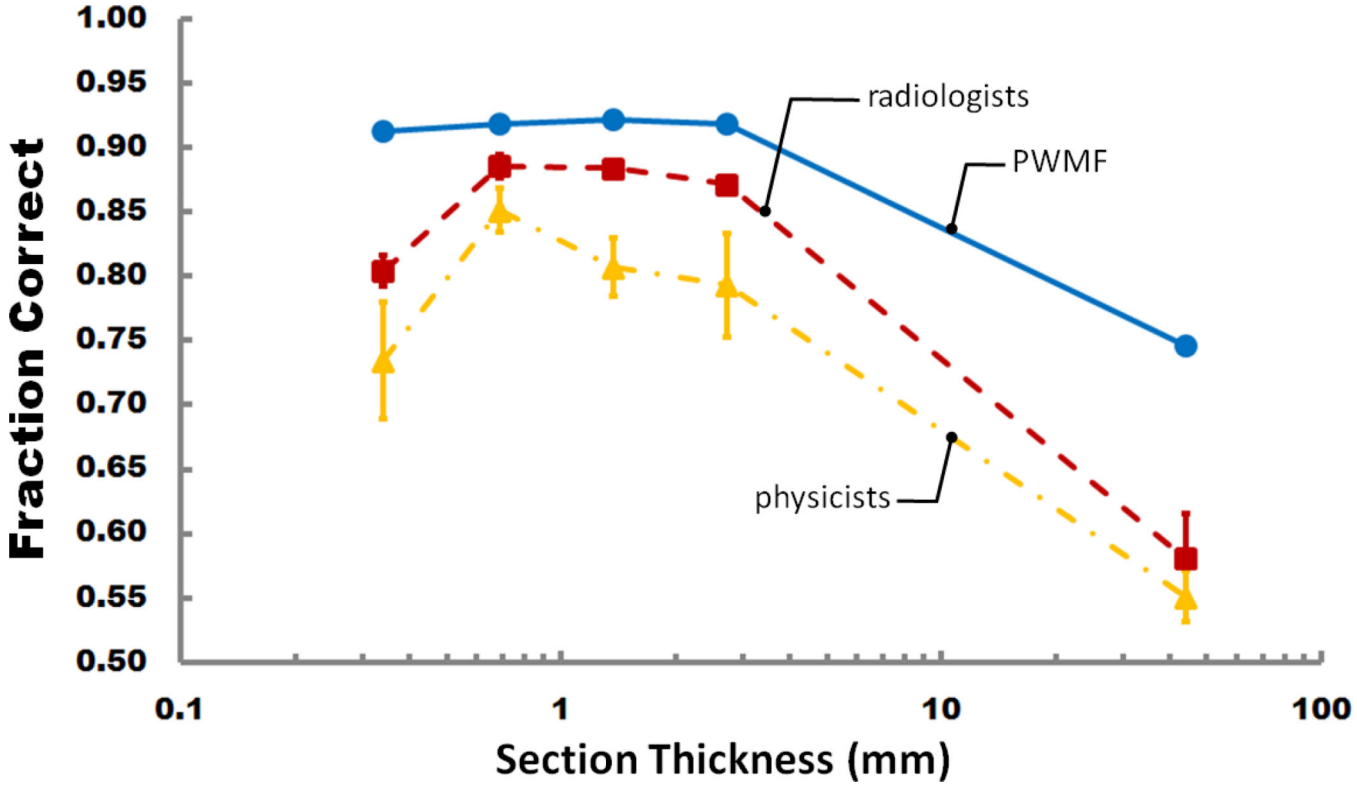

Figure 5.

Observer performance (average fraction of correct responses) for 2 mm diameter lesions is shown as a function of section thickness, for the PWMF (pre-whitened matched filter) observer, average radiologist observer, and for the average physicist observer. With the exception of the thinnest section thickness (0.33 mm) where performance is likely affected by quantum noise, there is a general decline in performance amongst all observers as the section thickness increases.